

Complex Bioelectric Impedance Measurement System for the Frequency Range from 5 Hz to 1 MHz

JAMES J. ACKMANN

Department of Veterans Affairs Medical Center and Department of Neurosurgery,
Medical College of Wisconsin, Milwaukee, WI

Abstract—Analytic techniques that have been successfully employed in materials science, and to a lesser extent in the study of biologic systems, have potential for improving the application of bioelectric impedance provided that both real and imaginary impedance components can be measured with sufficient accuracy over a given frequency range. Since biologic tissue, particularly animal tissue, is typically highly conductive, phase angles are small, making accurate measurements difficult. A practical four-terminal system employing commercial lock-in amplifiers is described and error sources and corrective techniques are discussed.

Keywords—Electric conductivity, Electronic instrumentation.

INTRODUCTION

Electrical impedance measurements have been used since the late 1800s to study the electrical properties of biologic tissue and to measure physiologic events. The methodology has been previously reviewed (1,4). While some investigations of tissue and cell suspensions have employed complex measurements, the majority of published studies have utilized only the absolute value or the real component. In contrast, in materials science research, numerous studies employing complex impedance measurements have been conducted and a significant methodology using complex-plane plotting techniques along with analytic methods has been developed; an overview of the methodology has been presented (7). The techniques can be extended to biologic systems provided that both real and reactive impedance components can be measured with sufficient accuracy over the frequency range of interest. Biologic tissue, particularly animal tissue, is typically highly conductive, and dissipation factors (defined as the ratio of the real component R to the reactive component X) are high; corresponding phase angles

($\tan^{-1} X/R$) are therefore small and obtaining the necessary data is not a trivial matter.

Instrumentation techniques for complex impedance measurements have been previously reviewed (1,7). The most commonly used technique applied to biologic tissue has been the two-terminal bridge; however, two major limitations of the technique limit applicability. Interfacial electrode impedance can be significantly greater than sample impedance and techniques permitting corrections, such as a variable-length conductivity cell, must be applied. The technique is limited to experiments in which a tissue sample can be introduced into the cell and is, in general, not applicable to studies in intact systems. Of equal importance is the inherent limitation of bridge methods in measuring impedances with high dissipation factors (7). While impedance analyzers are commercially available, these instruments are intended primarily for network and component analysis and are basically auto-balance bridges, which are subject to the same limitations noted above. Measurements are usually restricted to systems with dissipation factors of less than ten. In contrast, dissipation factors in animal tissue are frequently greater than 100 in the frequency range of interest. In addition, the measurement terminals of the instrument are configured as "four-terminal pairs," that is, the current and voltage terminals are connected internally, and the measurements are essentially two-terminal.

To eliminate electrode impedances from the measurement, a four-probe configuration in which a known measurement current is applied to a sample with one electrode pair, and the attendant voltage is measured with a second electrode pair, is frequently used. For complex measurements, a system capable of measuring both the amplitude and the phase of the measured voltage with respect to the applied current is required. This can be accomplished by a technique known as phase-sensitive detection. Commercial instruments, termed lock-in amplifiers, employing the method were introduced in 1972 and are used in a number of disciplines. Phase-sensitive detection is accomplished by sequential mixing and time-averaging operations. In addition to the signal to be mea-

Acknowledgment—This work was supported in part by the Department of Veterans Affairs Medical Center research funds.

Address correspondence to James J. Ackmann, Department of Neurosurgery, Medical College of Wisconsin, 9200 W. Wisconsin Avenue, Milwaukee, WI 53226.

(Received 4/22/91; Revised 1/29/92)

sured, a reference signal at the frequency of interest must be applied to the instrument. The reference is first converted to a square-wave; the signal to be measured, after suitable amplification, is then multiplied by the reference square wave. It is readily shown (7) that the resultant signal contains a DC term proportional to the amplitude of the input signal \times the cosine of the phase angle Θ between the reference and measured signal plus time-varying terms which are even harmonics of the reference signal; the latter components are removed with a low-pass filter. By internally shifting the phase of the reference signal by a known amount until a maximum DC output is obtained ($\cos \Theta = 1$), both the amplitude and phase of the input signal with respect to the reference can be determined. In some instruments, two square-wave reference signals, one in-phase and one at 90° with respect to the reference input, are generated internally and the multiplexing-filtering operation is performed with both reference signals to simultaneously measure both the in-phase and quadrature components of the input signal. By separate amplification of the two components, signals with real-to-reactive ratios of several hundred to one can be resolved. It is also readily shown (7) that the detection technique is highly frequency-selective with the exception of odd-order harmonics of the reference signal; these are attenuated by a factor of $1/n$ where n is the harmonic

number. Maximum input sensitivities are approximately $100 \mu V$ full scale.

When properly applied, a four-probe measurement system including a lock-in amplifier overcomes the limitations of bridge techniques: the effects of electrode impedance are minimized, measurements can be made in systems with high dissipation factors, and the frequency selectivity and sensitivity of the amplifier permit measurements in a noisy environment with small excitation currents. While conceptually simple, a number of factors can cause serious measurement errors. This communication describes a system consisting of two lock-in amplifiers along with ancillary circuits which are useful in the frequency range from approximately 5 Hz to 1 MHz in biologic tissue with dissipation factors up to approximately 200; the inherent error sources and system limitations are delineated. A Princeton Applied Research (PAR) Model 5204 lock-in amplifier is used in the range from 5 Hz-100 kHz and a PAR Model 5202 lock-in amplifier in the range from 100 kHz to 1 MHz.

ERROR SOURCES

A simple four-probe system using a PAR Model 5204 two-phase lock-in amplifier along with test results obtained in a physiologic saline bath are illustrated in Fig. 1.

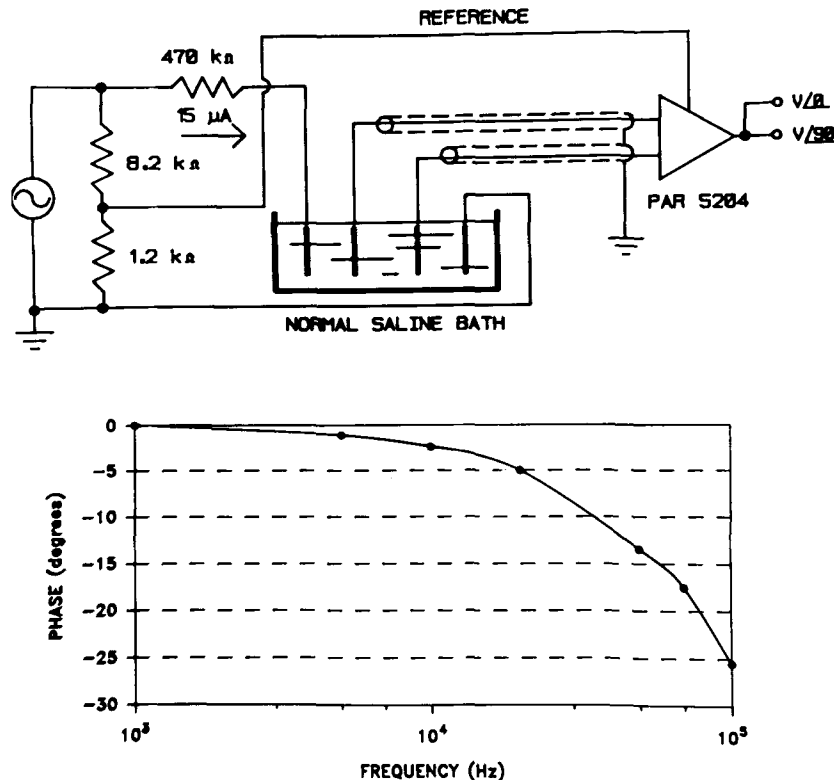


FIGURE 1. (Top) Basic four-probe impedance measurement system using lock-in amplifier; (bottom) phase errors.

A Wavetek Model 185 function generator, in series with a resistor significantly greater than the sample impedance, is used to deliver a sinusoidal constant current to the sample. The reference signal for the lock-in amplifier is derived from a voltage divider connected to the same oscillator. A second electrode pair is used to measure the resulting voltage. Assuming that the amplifier input impedance is infinite, the sample impedance between the sensing electrodes is computed as the ratio of the measured voltage to the applied current. Since both the real and quadrature components are measured, a complex computation can be made. The electrodes consist of four 0.3 mm diameter by 1 cm long platinum needle electrodes with 30 cm long leadwires mounted colinearly in a plastic substrate at 0.5 cm intervals and are submerged to a depth of 0.5 cm. Connection to the amplifier is made through 4-foot lengths of RG-59/U coaxial cable. Since a saline solution is purely resistive over a wide frequency range, measured phase should be zero. To apply impedance spectroscopy, maximum phase errors on the order of 0.2° are required; thus, the measured phase errors are clearly unacceptable. It should be noted that results are highly dependent upon lead placement and that virtually any set of data including positive phase errors can be obtained.

While errors may be analyzed by computing common-mode rejection ratios (10), error sources can be conveniently illustrated heuristically as in Fig. 2. In an ideal four-probe system, the impedance of the voltage sensing system is infinite; whereas, in a real situation, amplifier input impedance, stray capacitance, and input cable capacitance combine to present a finite impedance at the sensing electrodes. Due to imbalances in both capacitances and sensing electrode impedances, the leakage currents i_1 and i_2 of Fig. 2 will not in general be equal, resulting in a differential voltage at the amplifier input terminals. In studies of biologic systems which have high conductivity, the resulting phase errors can be particularly trou-

blesome. Also in an ideal system, the output impedance of the current source is infinite but in a real situation is finite. Conceptually, the current source output divides between the sample and the equivalent output impedance; with increased impedance in the loop containing the sample, a larger portion of current is diverted through the output impedance. Depending on the output capacitance, sample impedance, and electrode impedances, and how these change with frequency, significant phase errors can result.

Since surprisingly small stray capacitances coupled with electrode impedances can cause large phase errors, the capacitances and sensing electrode impedances Z_3 and Z_4 depicted in Fig. 2 were manipulated both experimentally and by means of an equivalent circuit model to provide a more quantitative assessment. Using the same experimental configuration as that for Fig. 1, electrode leadwires and input cables were arranged to obtain a minimum phase error. To simulate increased stray capacitance, an additional 4-foot length of RG-59/U cable was inserted into either the positive or negative amplifier input terminal, and to simulate electrode imbalances, a $100\ \Omega$ resistor was inserted in series with either the positive or negative voltage-sensing electrode leadwire. Results are illustrated in Fig. 3. Depending on experimental conditions, both positive and negative phase errors may be encountered and unacceptable errors can occur at frequencies as low as 5 kHz.

To quantify the magnitude of errors that can be expected for given parameters, an equivalent circuit model of the Fig. 1 test configuration was constructed using the linear circuit analysis program LINCAD (2) implemented on a VAX computer. Sample impedance was modeled with a $12\ \Omega$ resistor. Amplifier input impedance was modeled with a $100\ \text{M}\Omega$ resistor shunted by a $25\ \text{pF}$ capacitor according to manufacturer's specifications. Combined input cable and stray capacitances were represented with $150\ \text{pF}$ capacitors; these were alternately increased to

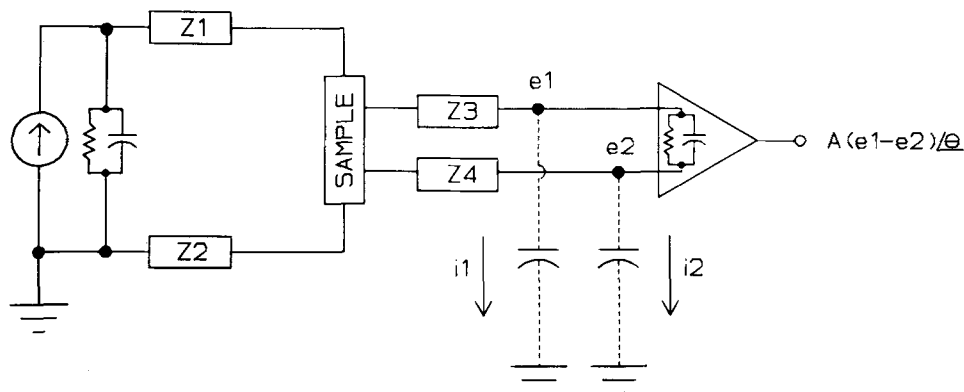


FIGURE 2. Error sources in basic system.

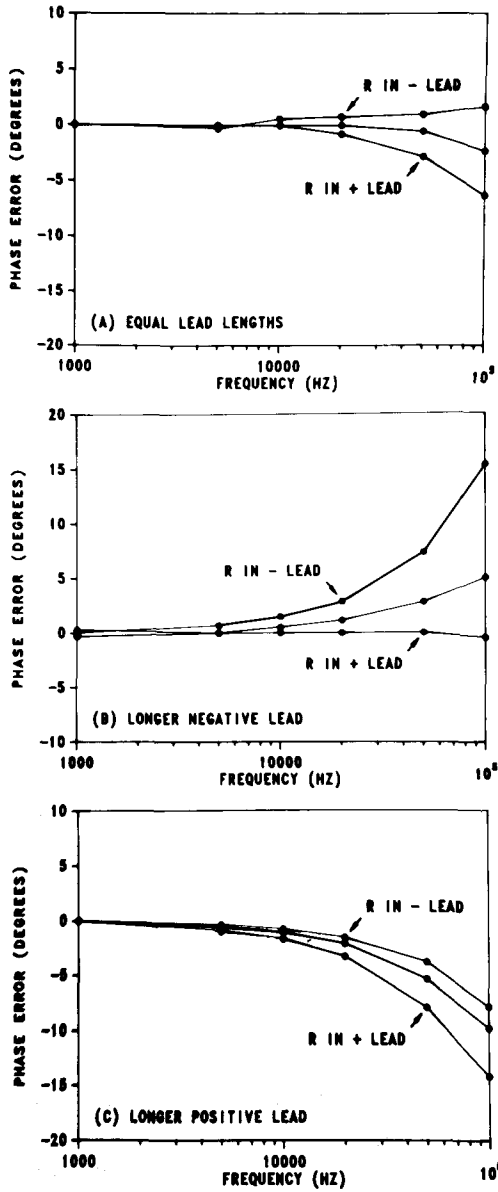


FIGURE 3. Experimentally determined phase errors as function of imbalanced cable capacitances and electrode impedances.

270 pF to simulate an increased input cable length. Electrode impedances were modeled by a parallel combination of a 1.25 μf and 25 k Ω resistor in series with a 100 Ω resistor; these values approximate experimental data previously obtained for the electrodes used. The 100 Ω value was increased to 200 Ω to simulate an electrode imbalance; this value is also consistent with previous data obtained during a study of electrode variability. The model was exercised according to the conditions previously described for Fig. 3 and resulting phase errors are shown in Fig. 4.

There is general agreement between experimental and model results, and no attempt was made to adjust model

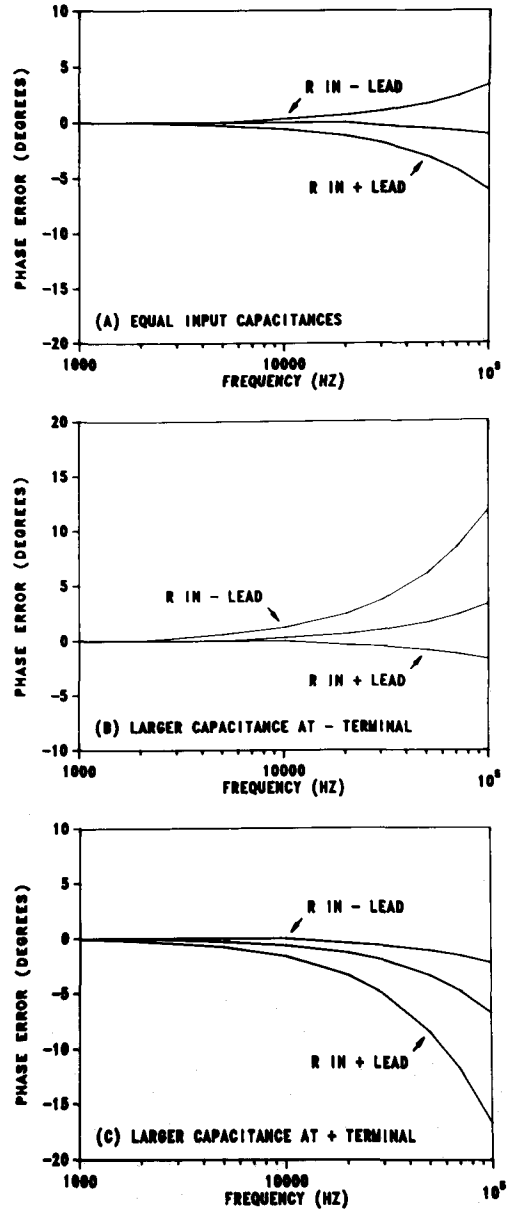


FIGURE 4. Results of circuit model for data of Fig. 3.

parameters for closer correspondence. With balanced electrodes and leakage capacitances (Fig. 4a, center trace), phase error is -1.1° at 100 kHz and results primarily from the combined effects of sensing electrode impedance and amplifier input capacitance. Although not illustrated, error increases to -5.7° at 500 kHz and to -11.1° at 1 MHz. Thus, even under balanced conditions, an amplifier input capacitance as low as 25 pF can result in intolerable phase shifts. Imbalances in electrode impedances cause either additional positive or negative phase errors, depending upon which lead contains the higher impedance electrode. With imbalanced electrode impedances (Fig. 4b and 4c), errors are exacerbated; however, an in-

creased electrode impedance in the lead opposite to that containing the increased capacitance reduces the error.

In summary, direct application of a commercially available instrument for measuring complex bioelectric impedance will in general produce unsatisfactory results. Phase errors result from the loading effects of amplifier input capacitance and imbalances in capacitive leakage currents to ground. In addition, as subsequently discussed more quantitatively, load-dependent phase shifts can occur in a current source due to output capacitance.

The above problems may be minimized by the inclusion of additional circuitry: loading effects due to amplifier input capacitance can be greatly reduced by incorporating low input capacitance buffer amplifiers, loading effects due to voltage-sensing cable capacitance can be significantly lowered by the use of driven shields, leakage currents to ground can be largely eliminated by isolating the current source, and current-source output capacitance can be decreased by careful design.

CURRENT SOURCE

In a four-terminal system employing a lock-in amplifier, a common reference must be applied both to the current source and to the amplifier; however, to eliminate a return path for capacitive leakage currents (see Fig. 2), the current source must be isolated from ground. This may be accomplished in several ways.

In a previous design (6), the drive to the current source was isolated optically. While the circuit operated satisfactorily up to 100 kHz, phase shifts within the isolation circuitry were unacceptable at higher frequencies. A scheme employing two current sources in series was therefore used in subsequent designs. With reference to Fig. 5, if the currents from two sources in series, one operating at 0° and the second at 180° , are precisely balanced, the currents in the return lead cancel, effectively

isolating the overall source from ground. The feasibility of obtaining the necessary tracking to effect isolation was demonstrated in a previous project in our laboratories (9).

An individual current source may be assembled using a single operational amplifier in several different configurations. As in any operational-amplifier circuit, performance parameters are frequency dependent. Modest frequency-dependent phase shifts can be accounted for by calibration; however, corrections cannot be made for phase shifts secondary to changes in load impedance which occur because of finite source output capacitance. In an earlier project (6), several conventional single operation-amplifier circuits (8) all proved unsatisfactory and a discrete-component circuit was required. While improved performance can be obtained in an operational amplifier circuit with additional components (5), a convenient alternative is a single-chip operational transconductance amplifier. This component has the generic characteristics of an operational voltage amplifier except that the forward transfer characteristic is best described as a transconductance rather than voltage gain, and the output is current, not voltage. The magnitude of the output current is equal to the product of the transconductance and input voltage. A bias current is used to program the transconductance. While intended as a gain-controlled building block for various applications, a balanced dual current source can be simply constructed.

With reference to Fig. 6, a single chip containing a dual amplifier (CA3280) is used. Bias currents of approximately 1 mA are applied at pins 3 and 6 which establish transconductances of approximately 25 mS. The balance potentiometer permits matching of the two transconductances and thus output currents. Following attenuation, the input voltage is applied to the positive input of one amplifier and the negative input of the other, thus establishing output currents which are at 0° and 180° with respect to the input signal. For the component values

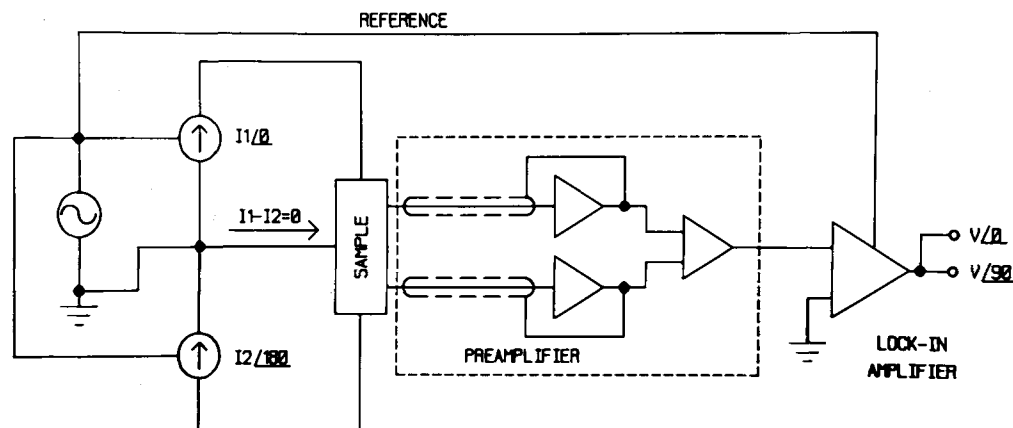


FIGURE 5. Practical four-probe system.

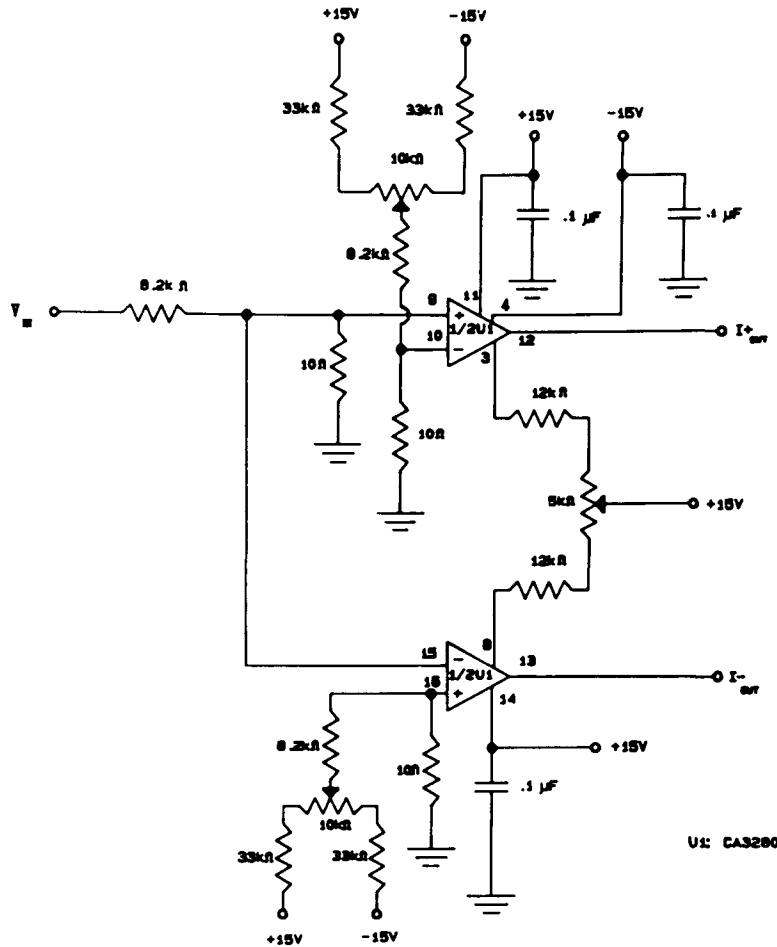


FIGURE 6. Current-source schematic diagram.

indicated, an output current of 30 μA RMS is produced with an input voltage of approximately 1.0 volt RMS. Separate DC offset adjustments are provided for each channel. The circuit was packaged on a printed circuit board contained in a 6.5 cm \times 7.5 cm \times 4.2 cm die-cast aluminum box. Miniature pin-jacks are provided for electrode connections.

Phase transfer characteristics as a function of load were determined experimentally and further evaluated by an equivalent circuit model using LINCAD (2). The output source was modeled by a voltage-dependent transconductance given by:

$$g_m(v) = 0.025 \frac{v}{1 + \frac{jf}{8.75(10^6)}} \quad (1)$$

The output source was shunted by a 3.3 M Ω resistor and 3.3 pF in accordance with measured values. Since the nominal output capacitance of the CA3280 per manufacturer's specifications is 7.5 pF nominal, and two sources are in

series, the capacitance value is reasonable. The input section was modeled by a 10 Ω , 8.2k Ω voltage divider per Fig. 6 with the amplifier input shunted by a 7 pF capacitor in accordance with specifications. The transconductance and corner frequency of the model were adjusted to provide a best fit to the actual data, but they also agree closely with nominal specified values. Both experimental and model results are illustrated in Fig. 7. While the frequency dependence of phase of the model agrees with actual data to only 800 kHz due to the simplified single pole representation, the phase change with load is well represented and clearly demonstrates the necessity of considering the effects of current source output capacitance.

Output saturation occurs approximately at the power supply voltages; thus, at current of 30 μA RMS (85 μA p-p), a total load of 350 k Ω can be driven.

BUFFER AMPLIFIERS

As previously discussed, loading effects of cable and amplifier input capacitance at the voltage-sensing termi-

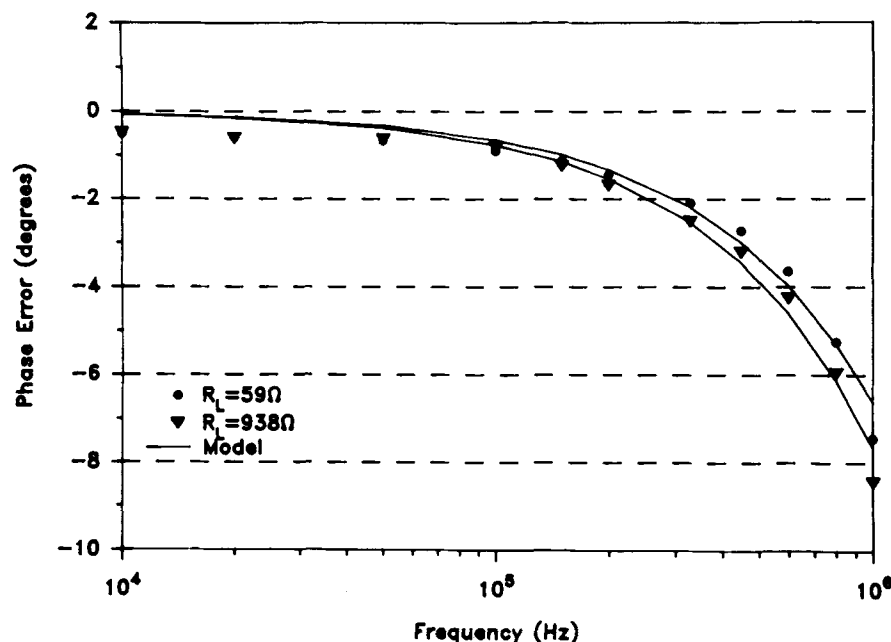


FIGURE 7. Current-source phase as function of frequency and load.

nals in a four-probe system can cause unacceptable phase errors. As indicated in Fig. 5, the use of unity-gain buffer amplifiers and shield drivers can minimize the problem. The buffer amplifiers provide a high impedance, low capacitance input. By maintaining the cable shield at the same voltage as the input, current flow between the shield and center conductor, except for distributed effects, is significantly reduced, thereby reducing the effective cable capacitance. The concept is usually applied by driving shields at the common-mode voltage of a differential amplifier (5). In the design used here, the usual unity gain operational-amplifier configuration is generally unsatisfactory because of instability, and at least formerly, discrete component circuits employing field-effect transistors were required (6). In recent years, however, integrated-circuit buffer-amplifiers with satisfactory characteristics have become available.

The circuit illustrated in Fig. 8 employs LH0033 devices. R-C networks in the power supply connections provide current limiting and are configured according to manufacturer's recommendations. 220 Ω resistors in series with the input and with the connection to the shield are included to prevent oscillation and were determined empirically. The PAR 5204 lock-in amplifier used in the frequency range from 5 Hz–100 KHz has provisions for differential input and the buffer outputs could be directly connected; however, the PAR 5202 amplifier used at higher frequencies has a 50 Ω single-ended input. To provide an input for this instrument, a conventional differential-to-single ended convertor using an LH0033 high-speed operational amplifier is included. A gain of

5.0 was chosen as a compromise between stability and bandwidth. Precision resistors are used to maintain common-mode rejection without additional adjustment. The circuit was packaged on a printed circuit board contained in a 6.5 cm \times 7.5 cm \times 4.2 cm die-cast aluminum box. Input leads consist of 50 cm lengths of RG-174 coaxial cable terminated with miniature alligator clips. Amplifier characteristics were measured using the PAR 5204 and PAR 5202 lock-in amplifiers. Gain is essentially constant at 4.94 (buffer amp gain \approx 0.99) from 5 Hz–2Mhz. Phase characteristics are illustrated in Fig. 9. Input capacitance is estimated at 6 pf and was determined by changing source impedance, measuring the additional phase shift, and computing the value using an equivalent circuit model. Common-mode rejection ratios were estimated with a common-mode voltage of 10.0 volts peak-to-peak using an oscilloscope to measure output; computed values were -68 db, -74 db, -80 db, -74 db, -61 db, and -54 db at frequencies of 100, 1 kHz, 10 kHz, 100 kHz, 500 kHz, and 1 Mhz, respectively. Noise referred to the input is estimated as 75 μ V RMS using an oscilloscope measurement.

OVERALL SYSTEM CHARACTERISTICS AND LIMITATIONS

The individual sources of error inherent in the lock-in amplifiers, current source, and preamplifier combine to form an overall system error which is a function of frequency, sample impedance, and electrode impedance. Absolute magnitude and phase errors which depend only on frequency and not on load (sample impedance combined

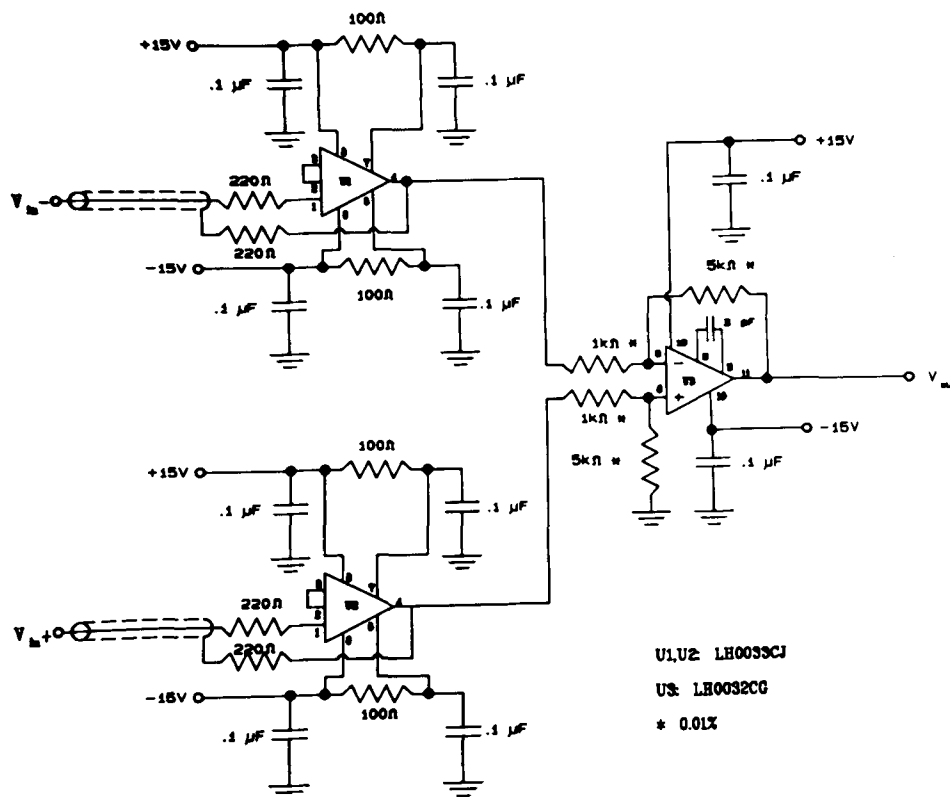


FIGURE 8. Buffer-amplifier schematic diagram.

with electrode impedance) can be accounted for and removed by calibrating the system with a known simulated sample. In practice, this accomplished with a low-capacitance precision resistor. The measuring current is applied to the resistor and the complex voltage (real and reactive components) measured at each of the desired measurement frequencies. Dividing the voltages by the calibration resistance results in an effective applied complex current. Experimentally determined voltages may then be divided by the effective current to yield the complex impedance. This procedure is effective to the extent that the calibration current is repeatable and that phase corrections are small with respect to experimentally determined values. Additional errors which result from load changes as well as system noise then determine the overall absolute accuracy.

Errors within the lock-in amplifier include both absolute phase error as well as phase noise. Absolute phase errors for the two instruments are illustrated in Fig. 10. The data were obtained using a 1.0 volt RMS sine-wave reference signal and a 15.0 mV input signal derived from a voltage divider connected to the same source; equivalent source impedance was approximately 50 Ω . The model 5204 phase was set to zero at 1 kHz and the model 5202 phase was set to zero at 200 kHz. As indicated, phase er-

ror for the Model 5204 is less than 1° and error for the Model 5202 is less than 3° over the useable frequency range of the system. After a 30-minute warmup period, readings are repeatable within the phase noise of the instruments. For the Model 5202, the manufacturer's specified noise is 0.035° peak-to-peak maximum over the entire frequency range of the instrument. For the Model 5204, specified noise is 0.005° peak-to-peak maximum at frequencies greater than 50 Hz. While not specified, noise at lower frequencies is substantially greater; measured values in the range from 5 Hz–100 Hz are illustrated in Fig. 11. The data were obtained by sampling the lock-in amplifier outputs at a rate of 2 samples/s with an analog-to-digital converter. It should be noted that the noise frequency is quite low; with reference to Fig. 10, the data for frequencies below 50 Hz were obtained by recording the lock-in amplifier outputs on a storage oscilloscope over a period of approximately two minutes and visually determining average values.

In addition to phase noise, settling time of the lock-in amplifiers must also be considered. For the Model 5204, the time required for reference lock with abrupt changes in reference frequency is less than two seconds at frequencies greater than 50 Hz; at lower frequencies, the required time depends on the initial frequency and the difference

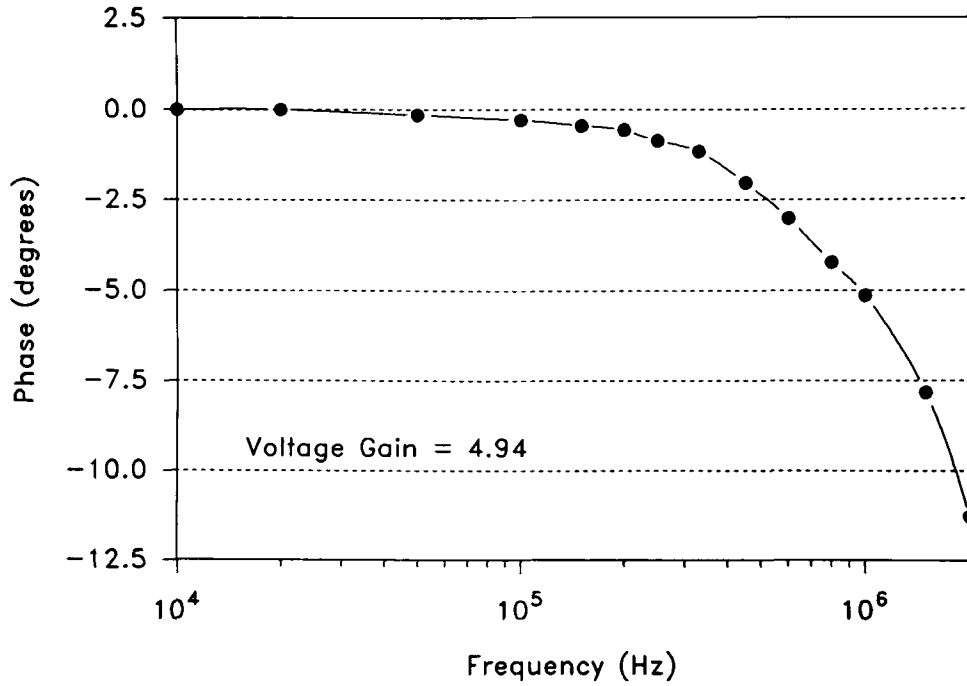


FIGURE 9. Buffer-amplifier phase vs. frequency.

between the initial and final frequencies. For example, the time required for reference lock for a change from 30 Hz–40 Hz is approximately 45 seconds and the time for a frequency change from 40 Hz–50 Hz is approximately 25 seconds. For the Model 5202 lock-in amplifier,

the settling time is less than 1 second for any changes over the entire operating range of the instrument.

An overall system calibration curve recorded with a 197.6 ohm resistive load is illustrated in Fig. 12. Current magnitude is 15 μ A RMS and is essentially constant with

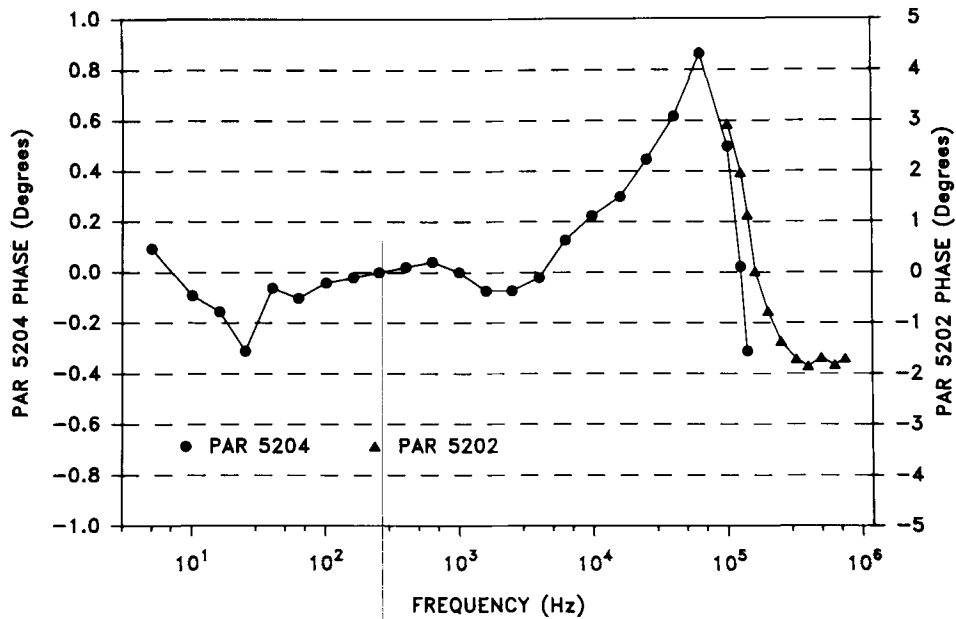


FIGURE 10. Lock-in amplifier phase characteristics vs. frequency.

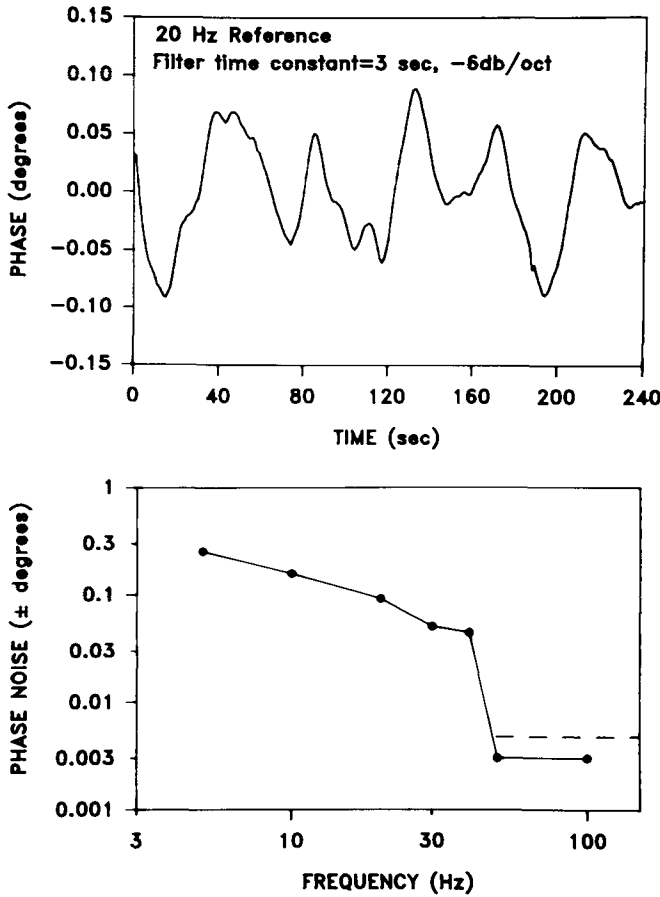


FIGURE 11. Phase noise at 20 Hz (top) and phase noise vs. frequency (bottom). Dashed line indicates specified maximum noise at frequencies above 50 Hz.

frequency; therefore, only phase is shown. Input to the preamplifier is approximately 3.0 mV and input to the lock-in amplifier is approximately 15 mV. Calibration phase is simply the sum of phase errors of the current source, preamplifier, and lock-in amplifiers. From approximately 10 kHz-100 kHz, the slightly negative phase shifts of the preamplifier and current source are balanced by the slightly positive phase of the lock-in amplifier (refer to Fig. 7, 9, and 10) and corrections are less than 1°. At higher frequencies corrections are larger due to increased negative phase of the current source and preamplifier. For a load range of 20 Ω - 500 Ω , the data of Fig. 12 are reproducible within the phase noise limits of the lock-in amplifier from 5-50 Hz, within $\pm 0.075^\circ$ between 50 Hz-100 kHz, and within $\pm 0.15^\circ$ from 100 kHz-1 Mhz. The reproducibility at frequencies lower than 50 Hz may be improved to approximately $\pm 0.15^\circ$ with time-averaging.

As previously noted, electrode impedances may result in further errors. To quantify these effects, resistors were inserted into all four system leads and the values required to cause an additional phase error of 1° at frequencies of 100 kHz, 200 kHz, 500 kHz, and 1Mz were determined; values were 1.5 k Ω , 750 Ω , 250 Ω , and 100 Ω , respectively. Electrode impedances decrease as a power function of frequency and impedances of electrodes typically employed in our laboratories (0.3 mm dia by 10 mm long platinum or stainless steel needles) are at least one order of magnitude less than the above values.

Measurements obtained on a two time-constant complex load, which simulates portions of data from an

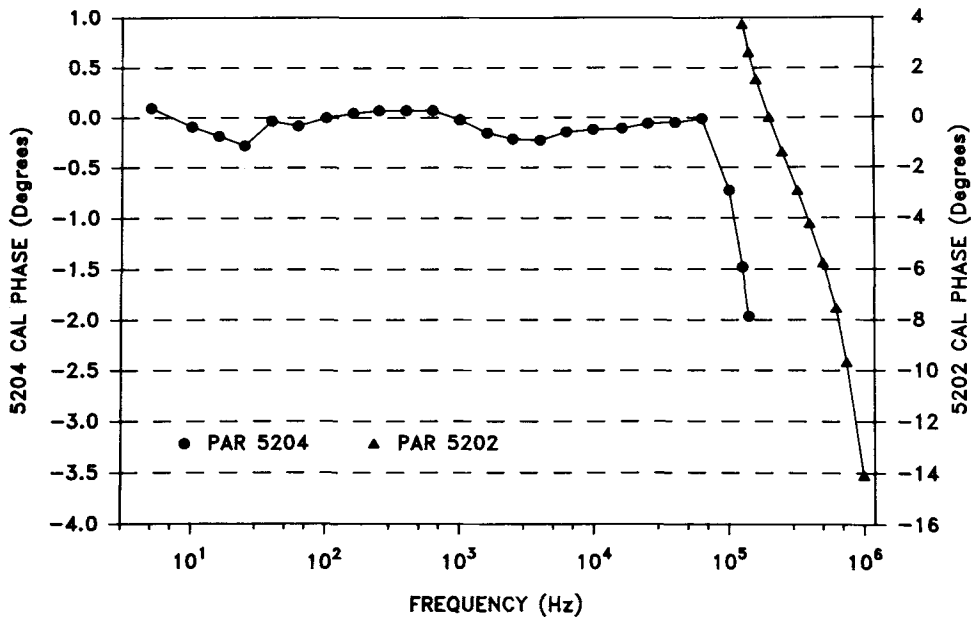


FIGURE 12. Calibration phase vs. frequency.

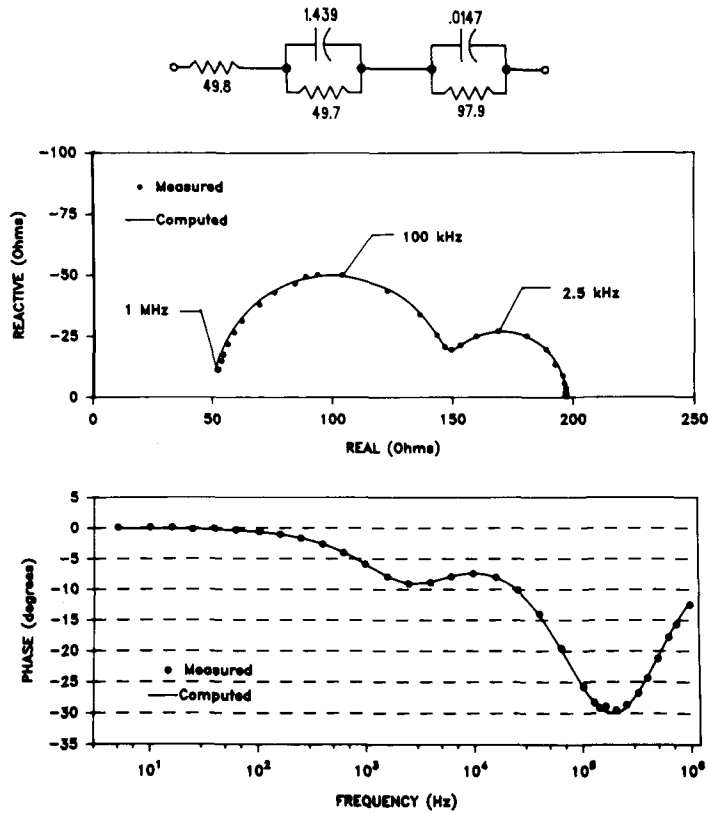


FIGURE 13. Impedance and phase vs. frequency plots for two time-constant circuits.

isolated lung preparation previously recorded in our laboratories (1), are illustrated in Fig. 13. Data were corrected using a calibration curve generated with a 197.6 Ω resistive load. To generate the computed curve, component values were measured using a Fluke Model 87 multi-meter.

Note that changes in the reactive component are well resolved in the frequency range up to 1 kHz where phase angles are less than 5°.

Finally, use of the system on a biologic specimen is illustrated in Fig. 14. The data are part of an investiga-

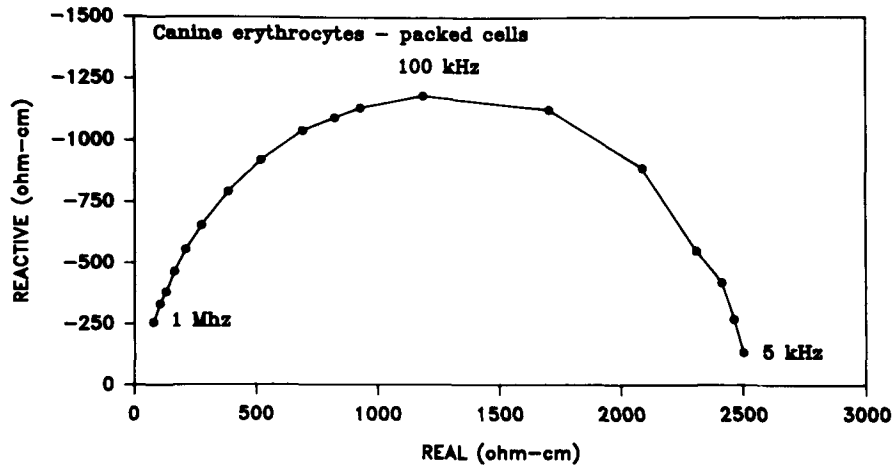


FIGURE 14. Complex resistivity plot of packed canine erythrocytes at 38.5°C.

tion of the complex resistivity of blood. Briefly, complex measurements were obtained from canine erythrocytes in plasma at various hematocrit using a 9 mm diameter cylindrical conductivity cell. Cylindrical current electrodes were spaced at 4 cm, and 0.5 mm dia voltage-sensing electrodes were embedded in the chamber wall at a separation of 1 cm. The data illustrated were obtained from packed cells. An analog circuit model of blood as a function of hematocrit can be constructed from the data and will be reported elsewhere.

DISCUSSION

Complex bioelectric impedance measurements may be accomplished in a number of ways with each method having advantages for a particular application. The four-probe system employing lock-in amplifiers described in this communication largely eliminates the problems associated with electrode impedances and stray capacitances at frequencies up to approximately 1 MHz. Data with sufficient accuracy to permit application of various materials-science analysis techniques can be obtained in systems with relatively high conductivity and resultant small phase angles. At frequencies above 50 Hz, data can be acquired at a rate of approximately one measurement every three seconds. At lower frequencies, acquisition time is substantially longer with settling times between frequencies of up to one minute. In addition, phase noise is considerably larger; if time-averaging is required to reduce the effects of phase noise, acquisition time could exceed two minutes per data point. The compliance of the current source is sufficient to tolerate a combined current-electrode impedance of approximately 350 k Ω at a measuring current of 30 μ A RMS, thus permitting measurements at relatively low frequencies, depending on electrode type. With the Model 5204 lock-in amplifier, measurements down to 0.5 Hz are possible; however, in our experience, settling time and phase noise render measurements below approximately 5 Hz impractical. Several amplifiers having a low frequency limit of 5 Hz and a settling time of approximately one-tenth that of the Model 5204 are available; however, the phase noise of these instruments is substantially greater up to frequencies of 1 kHz and has not proven practical in our experience.

It is emphasized that the impedance computation assumes that both the excitation current and measured volt-

ages are sinusoidal. Electrode impedances are a function of current density and this effect is frequency dependent with impedance decreasing as a power function of frequency (3). At low frequencies, electrode impedances can be extremely high and can potentially cause operation of the current source outside the linear range with resultant waveform distortion. While the lock-in amplifier is narrow-band (but does respond to odd harmonics of the reference) and would partially mitigate the error, the measured impedance would nonetheless be incorrect. It is therefore important to visually monitor the measured signal with an oscilloscope; in the PAR Model 5204, a signal monitor jack is provided for this purpose. With the electrodes and current densities (<0.3 mA/cm²) employed in our studies, no problems have been encountered with frequencies as low as 5 Hz.

REFERENCES

1. Ackmann, J.J.; Seitz, M.A. Methods of complex impedance measurements in biologic tissue. *CRC Crit. Rev. Biomed. Eng.* 11:281-311;1984.
2. Cornet, W.H.; Batocletti, F.E. *Electronic circuits by system and computer analysis*. New York: McGraw-Hill; 1975.
3. Geddes, L.A. *Electrodes and the measurement of bioelectric events*. New York: John Wiley and Sons; 1972.
4. Geddes, L.A.; Baker, L.E. *Principles of applied biomedical instrumentation*. New York: Wiley-Interscience; 1975.
5. Graeme, J.G. *Applications of operational amplifiers: Third-generation techniques*. New York: McGraw-Hill; 1973.
6. King, M.A. *A four-terminal instrumentation system for the measurement of complex bioelectric impedance*. Milwaukee: Marquette University; 1978. MS Thesis.
7. Macdonald, J.R. *Impedance spectroscopy*. New York: John Wiley and Sons; 1987.
8. Millman, J.; Halkias, C.C. *Integrated electronics*. New York: McGraw-Hill; 1972.
9. Smith, G.A. *Analysis of the current pathways associated with multifrequency impedance measurements of the lung*. Milwaukee: Marquette University; 1982. MS Thesis.
10. Winter, B.B.; Webster, J.G. Reduction of interference due to common mode voltage in biopotential amplifiers. *IEEE Trans. BME* 30:58-62;1983.

NOMENCLATURE

- g_m = transconductance
 V = voltage
 f = frequency
 j = $\sqrt{-1}$